Journal of Power Sources 196 (2011) 3790–3802

Contents lists available at ScienceDirect

Journal of Power Sources

journal homepage: www.elsevier.com/locate/jpowsour

High-fidelity stack and system modeling for tubular solid oxide fuel cell system design and thermal management

K.J. Kattke[a], R.J. Braun[a,*], A.M. Colclasure[a], G. Goldin[b]

[a] Division of Engineering, Colorado School of Mines, 1610 Illinois Street, Golden, CO, USA
[b] ANSYS-FLUENT, Lebanon, NH 03766, USA

ARTICLE INFO

Article history:
Received 12 November 2010
Received in revised form
14 December 2010
Accepted 16 December 2010
Available online 24 December 2010

Keywords:
SOFC
System analysis
Modeling
Thermal management
Stack design
CFD

ABSTRACT

Effective thermal integration of system components is critical to the performance of small-scale (<10 kW) solid oxide fuel cell systems. This paper presents a steady-state design and simulation tool for a highly-integrated tubular SOFC system. The SOFC is modeled using a high fidelity, one-dimensional tube model coupled to a three-dimensional computational fluid dynamics (CFD) model. Recuperative heat exchange between SOFC tail-gas and inlet cathode air and reformer air/fuel preheat processes are captured within the CFD model. Quasi one-dimensional thermal resistance models of the tail-gas combustor (TGC) and catalytic partial oxidation (CPOx) complete the balance of plant (BoP) and SOFC coupling. The simulation tool is demonstrated on a prototype 66-tube SOFC system with 650 W of nominal gross power. Stack cooling predominately occurs at the external surface of the tubes where radiation accounts for 66–92% of heat transfer. A strong relationship develops between the power output of a tube and its view factor to the relatively cold cylinder wall surrounding the bundle. The bundle geometry yields seven view factor groupings which correspond to seven power groupings with tube powers ranging from 7.6–10.8 W. Furthermore, the low effectiveness of the co-flow recuperator contributes to lower tube powers at the bundle outer periphery.

1. Introduction

Small-scale SOFCs are becoming increasingly attractive over conventional technologies in several applications. For portable power, SOFCs are predicted to have higher energy densities than batteries for applications that require long operational times or mission durations. In auxiliary power applications, the high potential efficiency of SOFC technology outweighs their added cost in comparison to conventional small-scale diesel generators. For many potential applications, small-scale SOFC systems become most attractive when operating at efficiencies exceeding 40%-LHV. High system efficiency is only realized when the SOFC stack and balance of plant (BoP) are effectively integrated. Strategic coupling of sinks and sources of thermal energy ensures thermally self-sustaining operation and reduces the need to supply excess fuel to the system for preheating flow streams. Identification of thermal sources and sinks within the system necessitates the need for a system-level SOFC model that accounts for thermal interactions occurring between components.

The cell-stack in small-scale SOFC systems is typically in close proximity to BoP components and depending on packaging and cell geometry, introduces a strong thermal interaction with adjacent components. This is often the situation for tubular-based SOFC systems where because of the coupling, a change in SOFC performance alters process statepoints throughout the system and vice versa. Furthermore, adequately capturing the physics of such geometries necessitates an understanding of the convective flow field within the bundle. Reliable prediction of stack performance in small-scale tubular SOFC systems therefore requires a model that is also inclusive of thermofluidic interactions between system components.

System design and simulation models found in the extant literature typically employ approaches that either (i) impose adiabatic boundaries on all system components [1], (ii) employ thermodynamic models to predict the required heat loss from components based on a given inlet and outlet state [2], or (iii) calculate component heat losses without any thermal coupling [3–5]. These approaches neither capture the thermofluidic interactions between components nor do they quantify the effect thermal coupling has on system performance. When operating at elevated temperatures (500–1000 °C), some degree of thermal interaction amongst SOFC components occurs even for instances where each component may be wrapped in insulation. Significant thermal interaction is typically found in high volumetric power density portable and mobile

* Corresponding author. Tel.: +1 303 273 3055; fax: +1 303 273 3602.
E-mail addresses: kkattke@mines.edu (K.J. Kattke), rbraun@mines.edu (R.J. Braun).

0378-7753/$ – see front matter © 2010 Elsevier B.V. All rights reserved.
doi:10.1016/j.jpowsour.2010.12.070

SOFC systems in the 1–10 kW range. Additionally, containment of system thermal energy in such systems becomes more difficult as the ratio of surface area-to-volume increases. In such systems, compactness is a premium and once robust operability is achieved, bulky insulation may be foregone in favor of a more compact system. Kattke and Braun [6] have previously generated system models that incorporate component interactions for small, mobile planar SOFC systems using relatively simple thermal resistance approaches. While such approaches can be effective for systems that contain primarily thermal interactions (i.e., there is limited dependence on the flow field external to the device), they are more limited for tubular geometries that have both high degrees of thermal and fluidic coupling.

The objectives of the current work are to (i) create a steady-state, high-fidelity cell-stack model able to predict performance variations amongst cells, (ii) create a thermally coupled system model around the high-fidelity cell-stack to capture the thermal and fluidic coupling throughout the system, (iii) use simulation results to suggest improved system designs, (iv) and provide cell performance groupings to increase the accuracy of reduced-order models. The SOFC system model includes a tubular SOFC stack, catalytic partial oxidation (CPOx) fuel reformer, tail-gas combustor (TGC), recuperator, and all process flow conduits. In this paper, we first present the overall modeling approach and system geometry under study. Next details on the CFD computational domain, user-defined function, individual component models, and information exchange between models is given. The capabilities of the system simulation tool are explored on a prototype 66-tube SOFC system design with an output power range of 500–1000 W [7].

2. Modeling approach

The level of model fidelity applied varies throughout the system model. Electrochemistry, anode fluid dynamics, and heat transfer within the tube bundle is captured through a previously developed 1-D electrochemical tube model [8]. Unlike planar stacks where relatively uniform anode and cathode gas flows exist in small length scale flow channels, tubular stacks posses relatively large flow areas external to the tubular cells where spatial flow variations can occur. The tube bundle geometry under investigation is shown in Fig. 1, where the anode gas flow is internal (tube-side) to and cathode gas flow is external (shell-side) to the cells. A large cathode flow area leads to spatial variations in fluid flow, temperature, and oxidant concentration. The need to accurately capture spatial property variations within the cathode due to thermofluidic interactions is the main motivation for incorporating a computational fluid dynamics (CFD) model of the cathode gas volume as shown in Fig. 1.

Each tubular cell in the stack is modeled with a one-dimensional (1-D) electrochemical tube model that is coupled to the three-dimensional (3-D) CFD flow field. Modeling of the SOFC stack alone is not sufficient for the purposes of stack design because of a large performance coupling between BoP and the stack. Feedback between BoP components and the stack is required. Coupling BoP models to the stack model provides the needed feedback for a realistic system modeling tool. The CFD computational domain includes the cathode (shell-side) gas flow, a tail-gas recuperator, the CPOx fuel/air preheat tube region, and stack endplates. The CPOx and TGC components and their surrounding geometries are modeled with quasi-one dimensional thermal resistance models that are coupled to both the CFD and tube models. All models are interconnected through passing of thermodynamic states and heat transfer rates at intersecting model boundaries (see Fig. 3). Details on system geometry are given in Section 2.1 followed by the details of each component model and their coupling to create the system modeling tool, Sections 2.2–2.5.

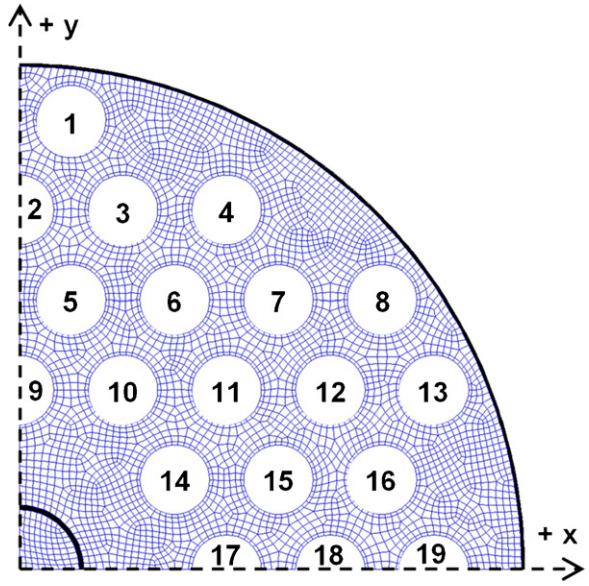

Fig. 1. Top view of 66-tube stack arrangement. CFD grid surrounds the domain of the tube model. Each cell is modeled independently with the tube model. Central tube is for fuel/air preheating.

2.1. System model geometry

The system design under investigation is derived from a patent application by an SOFC developer for a portable power system [7]. The patented stack is of tubular geometry with 36 tubes arranged in a hexagonal grid. The system, depicted in the simplified diagram of Fig. 2, can be generalized as a centrally located stack surrounded by larger cylindrical cans creating annular process flow channels. The entire system is wrapped in insulation and operates as described below.

First, oxidant for the cathode enters the system through four inlet tubes at the top of the insulation. Oxidant is then preheated in a three-fluid (oxidant, cathode gases, TGC exhaust) annular recuperative heat exchanger. Leaving the recuperator, oxidant turns radially inward entering the cathode. Oxidant leaves the cathode through concentric circle cut-outs surrounding each tube in the outlet tube-sheet. Fuel entering the system is first sent through an atomizing spray nozzle mixing with air at the upper outside edge of the insulation. The fuel/air mixture is preheated as it flows down a centrally located tube before entering the CPOx reformer. Leaving the reformer, reformate is distributed inside a fuel plenum located directly beneath the inlet tube-sheet. Reformate enters the anode gas channels and flows up toward the outlet tube-sheet. Anode and oxidant gases leaving the stack mix directly above the outlet tube-sheet and enter the TGC. TGC exhaust gas flows radially outward, turns 90°, and flows down an annular channel in the recuperator. Exhaust gas leaves the recuperator and is funneled radially inward and is expelled from the system through conduits at the bottom of the insulation.

In order to simulate a system of more applicable power capacity, the 36-tube patent application design was scaled to a system with a nominal power output of 650 W. The scaled 650 W system began with a 66-tube bundle geometry provided by the developer. The cells are arranged in a hexagonal grid that is symmetric about the *x*- and *y*-axes as shown in Fig. 1. In the symmetric tube bundle, there are 19 distinct tubes as labeled in Fig. 1. BoP components including the recuperator, CPOx, and TGC are scaled from the 36-tube system to fit around the larger 66-tube stack. Scaling the recuperator gas channels began by attempting to maintain a constant Reynolds number between the 36 and 66-tube systems. Equating Reynolds

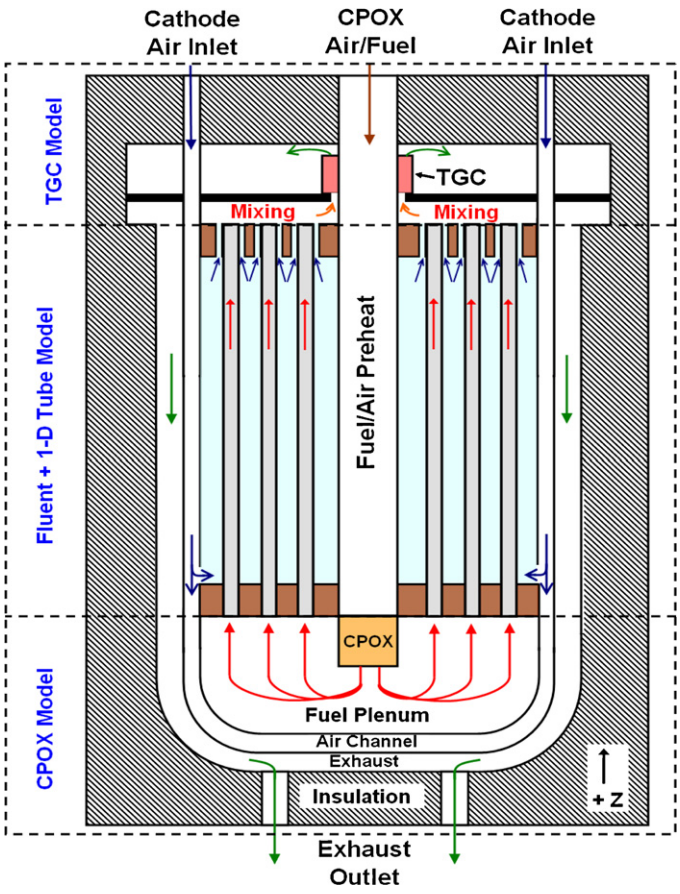

Fig. 2. System model geometry. Dashed lines illustrate domain of component models.

numbers simplifies to Eq. (1) as density and viscosity are constant between the two systems. Examining the air channel of the recuperator, the inner radius is set by the outer radius of the 66-tube bundle leading to a larger hydraulic diameter, D_h, than in the smaller 36-tube system. The 66-tube system also operates with approximately nine times more airflow (i.e. increased velocity, U) which requires a very large channel to maintain a constant *Re #*.

$$\frac{Re_{66}}{Re_{36}} = \frac{D_h U\big|_{66\,\text{tubes}}}{D_h U\big|_{36\,\text{tubes}}} = 1 \tag{1}$$

As an alternative scaling method, the gas channel widths within the recuperator, CPOx, and TGC of the 66-tube system are set equal to the channel widths in the 36 = tube system. The result is a nominal 650 W system centered around a 66-tube stack with a system architecture equivalent to the 36-tube system, Fig. 2.

Details of reactor sizing in the CPOx and TGC along with the tubular cell length, diameter, and thickness were extracted from information provided by the developer. The resulting system dimensions are shown in Table 1. Inlet flow conditions to the nominal 650 W system were also supplied by the developer.

Table 1
System and tubular cell dimensions, units in [cm].

	Height	OD	Ins. thickness
CFD domain	12.8	22.6	3.0
CPOx	6.3	22.6	2.4
TGC	5.8	21.6	3.2
System	24.9	22.3	2.9 (avg)
SOFC cells	12.5 (active)	1.1	–

2.2. Computational fluid dynamics model

The CFD software platform employed in the model development was ANSYS® FLUENT®. It is also the FLUENT software that executes a User Defined Function (UDF) which integrates all component models. In the subsequent sections, the FLUENT domain, settings, and the UDF are discussed.

2.2.1. Domain

The domain of the CFD model is illustrated in Fig. 2 which includes the entire cathode and stack endplates along with the majority of the recuperator, fuel/air preheat flow, and system insulation. The outer diameter (cathode surface) of every tubular cell represents the boundary between the CFD and tube model. FLUENT solves the mass, energy, momentum, and species conservation equations within the computational domain of the CFD model. Owing to the stack symmetry (see Fig. 1), one-quarter of the system is modeled with symmetry boundary conditions applied at the *x*- and *y*-axes.

2.2.2. CFD model settings

Solid conduction, convection, and radiation heat transfer mechanisms are modeled throughout the CFD domain. Assuming all gas species are transparent and non-participating, a surface-to-surface radiation model is most applicable, but surface-to-surface is unavailable in FLUENT with symmetry boundary conditions. Alternatively, a discrete ordinates radiation model is utilized. With all fluids set as transparent, discrete ordinates acts as a surface-to-surface radiation model. To check the validity of the discrete ordinates method, a complete 66-tube CFD model with surface-to-surface radiation was simulated. A comparison of numeric results between surface-to-surface and discrete ordinates methods found excellent agreement.

Diffusion occurs within the CFD domain as oxygen is reduced at the cathode electrode surface (outer diameter of cells). The flux of O_2 diffusion to the cathode surface is predicted with the 1-D tube model. Diffusion from the bulk cathode gas is modeled using Fickian diffusion utilizing temperature dependent binary diffusion coefficients, D_{ij}. Since the cathode is a two species mixture, $D_{O_2,m} = D_{O_2,N_2}$ and $D_{O_2,N_2} = D_{N_2,O_2}$ where m is the mixture. The temperature dependent polynomial fit to the binary diffusion coefficient, D_{O_2,N_2}, was calculated with Cantera [9].

$$D_{O_2,N_2} = 1.095 \times 10^{-10} \cdot T^2 + 7.993 \times 10^{-8} \cdot T - 1.1559 \times 10^{-5} \tag{2}$$

where T is in Kelvin.

A laminar flow solver is used throughout the CFD domain which is appropriate because the largest Reynolds number in the flow field is estimated at approximately 1200.

Piecewise-linear temperature dependencies of density, specific heat, thermal conductivity, and viscosity are used for each gas species. Thermal conductivity and viscosity use a mass weighted mixing law while the density is calculated using the incompressible ideal gas law.

Solid materials used within the CFD domain include a metal, insulation, and the SOFC tube material. Metal components include the inlet and outlet tube-sheets, stack can wall, fuel/air preheat tube, and the recuperator wall separating air and exhaust flows. All metals are modeled as INCONEL® 600 alloy with thermal conductivity applied as a piece-wise linear function extracted from manufacturer data [10]. Thermal conductivity values range from 17.3 to 27.5 $W\,m^{-1}\,K^{-1}$ in the temperature range of interest. An emissivity of 0.9 is applied to all metal surfaces and is representative of an oxidized INCONEL® 600 alloy [10]. The insulation around the system is modeled as fiberboard with a thermal conductivity

applied as a 2nd order polynomial fit of manufacturer data [11], as shown below. An emissivity of 0.9 is assigned to all insulation surfaces.

$$k_{fb} = 2.857 \times 10^{-8} \cdot T^2 - 2.743 \times 10^{-6} \cdot T + 2.002 \times 10^{-2} \quad (3)$$

A common thermal conductivity, 10.5 W m^{-1} K^{-1}, is applied to the tube solid in the CFD model and 1-D tube model. A precise emissivity of SOFC cathodes is uncertain; therefore, an emissivity value consistent with the literature is used, $\varepsilon_{tube} = 0.8$ [12,13]. Sensitivity analyses have revealed radiation heat transfer to be relatively insensitive to surface emissivities because all radiation exchange occurs within relatively small enclosures.

2.2.3. User Defined Function (UDF)

A UDF written in C employing FLUENT built-in functions is used to thermally integrate the CFD model to the remaining SOFC system. All CFD boundaries except the outer insulation surface represent interfaces with either the 1-D tube model, the CPOx model, or the TGC model. The outer diameter of every tubular cell represents the boundary between the CFD model and the 1-D tube model. The top and bottom of the CFD domain represent the boundaries between the TGC and CPOX models, respectively. It is the UDF that provides the communication pathways between FLUENT and the component models. A schematic of the required system model connections is shown in Fig. 3.

The UDF is called within FLUENT at the start of every FLUENT iteration and thermally couples all components at their common boundaries. Passing of information from one model to another at their intersections occurs via the writing and reading of data files. As an example, the thermodynamic state of fuel/air leaving the CFD domain is extracted with the UDF and written to a data file which the CPOx model reads as the inlet to the CPOx reformer. While the UDF relays boundary conditions to the CFD model every FLUENT iteration, executing the 1-D tube model, CPOx model, and TGC model occurs every N FLUENT iterations to update these boundary conditions. The current modeling strategy is to set $N = 5$, but this is an input parameter that could be optimized to reduce computational time.

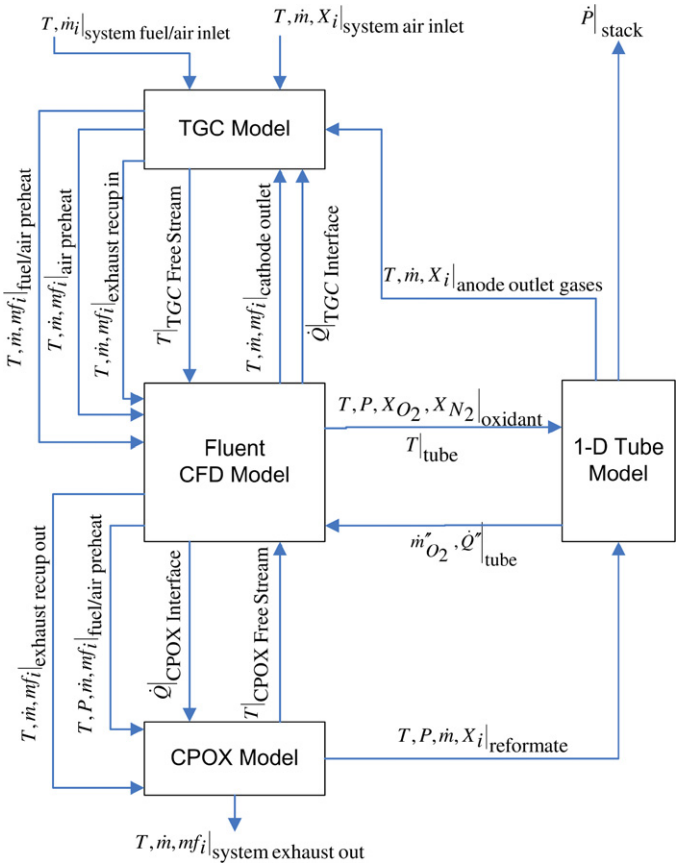

Fig. 3. Communication pathways required between all component models. Passing of information conducted by UDF.

2.3. 1-D electrochemical tubular cell model

A previously developed 1-D anode-supported tube model is employed to model the electrochemically active cell regions [8]. The model incorporates electrochemistry, anode gas flow, and heat transfer within the anode flow channel and tube solid. Gas diffusion within the porous anode is modeled using the Dusty-gas model. Electrochemical performance is based on the Nernst equation with cathode and anode activation losses, concentration losses, and ohmic losses. Axial conduction is assumed to occur within the relatively thick anode structure only.

Each tube extends from the bottom of the inlet tube-sheet to the top of the outlet tube-sheet. Electrochemically active cell area is defined by the tube area between the tube-sheets. More specifically, the tubes are electrochemically inactive within the space where the tubes protrude into the tube-sheet because tubes are being supported by the tube-sheet. In the case of the *inlet* tube-sheet, no oxidant reaches the cathode surface and because ion conduction is primarily normal to the tube (not axial) the surface is assumed inactive. In contrast, tubes are assumed electrochemically inactive within the *outlet* tube-sheet even though oxidant flow reaches the cathode surface. This is a valid assumption because the 3.2 mm thickness of the tube-sheets is small in comparison to the 125 mm active tube length. Modeling of the entire bundle is accomplished by simulating every tube in the bundle with the 1-D tube model.

2.4. Coupling 3-D CFD domain to 1-D tube model

The approach to couple the 3-D CFD cathode to the 1-D tube model is discussed in the following. The coupling process is carried out within the UDF.

2.4.1. Mapping 3-D mesh to 1-D bands

In all cases considered, the CFD computational grid of the cathode at the tube boundaries is finer than the 1-D band discretization used within the tube model as illustrated in Fig. 4. The first step in the mapping process is to number each 1-D tube band in order of increasing axial location. A common band grid is used on every tube within the bundle. Next, the axial locations of the 1-D band edges are calculated. Then, a loop begins over all FLUENT control volumes that border a tube wall. In this loop, the centroid of the control volume is first calculated. The control volume is then mapped to the

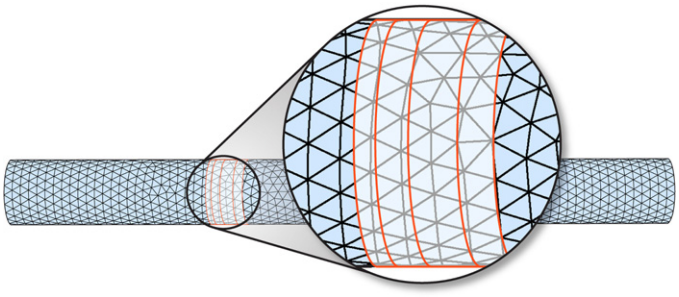

Fig. 4. Fluent discretization at SOFC tube interface overlaid on 1-D tube model bands.

tube band whose edges bound the control volume centroid in the axial direction. This procedure results in a mapping between the 3-D CFD grid and the 1-D bands of the tube model. This mapping is used to pass information between the CFD and tube models.

2.4.2. Variable passing

As shown in Fig. 3, the UDF passes the variables required for a complete coupling of mass and energy between the CFD and 1-D tube model. FLUENT provides the thermodynamic state of oxidant in the control volumes adjacent to the tube wall boundary as well as the temperature at the tube surface to the tube model. The tube model provides the resulting heat and oxygen flux occurring at the tube surface.

All flow variables extracted from FLUENT are first area-averaged amongst all control volumes within their assigned axial band, thus creating area-averaged 1-D profiles that the tube model can interpret. Every FLUENT-passed variable is then sent to the tube model *except for the tube temperature profile*.

2.4.2.1. Tube temperature smoothing. Tube temperature profiles must be smoothed before they are applied as boundary conditions in the tube model. Due to area averaging, the first derivative of tube temperature is not smooth, that is step changes in tube axial conduction result if the area averaged tube temperature is applied directly in the 1-D tube model. Tube axial conduction profiles are smoothed by fitting an nth order polynomial to the area-averaged tube temperature data. An axial tube temperature profile extracted from the nth order polynomial fit is applied to the tube model.

2.4.2.2. Interpolating 1-D tube in CFD model. All 1-D tube model variables passed to Fluent are applied using linear interpolation. As an example, the value of heat flux applied to a particular Fluent control volume is determined with the linear interpolation scheme illustrated in Fig. 5 and given by Eqs. (4) and (5),

$$\frac{z_c - z_1}{z_2 - z_1} = \frac{Q_c'' - Q_1''}{Q_2'' - Q_1''} \tag{4}$$

$$Q_c'' = \frac{z_c - z_1}{z_2 - z_1} \cdot \left(Q_2'' - Q_1''\right) + Q_1'' \tag{5}$$

where z_1, z_2 are the axial locations of the tube model band centers. z_c is the axial location of the centroid located on the tube wall face of FLUENT control volume c. Q_1'' and Q_2'' are the heat fluxes calculated via the tube model and Q_c'' is the heat flux applied to control volume c within the CFD model.

2.4.3. Boundary conditions in CFD model

The tube surface heat flux is applied directly as a heat flux thermal boundary condition at each tube wall in the CFD model. Oxygen flux is applied as a sink of mass and energy to each control volume that borders the tube walls, where each sink is calculated as:

$$\text{Mass Source} = \frac{\dot{m}''_{O_2,\text{face}} \cdot A_{\text{face}}}{V_{CV}} [=] \text{kg m}^{-3}\,\text{s}^{-1} \tag{6}$$

$$\text{Energy Source} = \frac{\dot{m}''_{O_2,\text{face}} \cdot A_{\text{face}} \cdot h_{O_2,\text{face}}}{V_{CV}} [=] \text{W m}^{-3} \tag{7}$$

where $\dot{m}''_{O_2,\text{face}}$ is the interpolated oxygen mass flux rate applied at a control volume bordering the tube wall boundary, A_{face} is the area of the tube wall face, V_{CV} is the volume, and $h_{O_2,\text{face}}$ is the enthalpy of oxygen in said control volume.

2.4.4. Electrochemically inactive tube ends

The electrochemically inactive tube ends within the tube-sheets are discretized and incorporated within the CFD domain. The conductive heat flux at the inlet and outlet of the electrochemically active tube length, calculated with the tube model, is applied as a heat flux boundary condition within FLUENT at the interface between the active and inactive tube sections. Anode gas flow in the non-reactive ends is not discretized in FLUENT and modeled within the CPOx and TGC models.

2.5. Modeling of fuel gas processing

Reforming of the liquid hydrocarbon fuel feed to the system occurs within the small CPOx unit that is integrated within the stack. Depleted anode fuel gases are completely oxidized in the tail-gas combustor which is located at the end of the tube bundle opposite of the CPOx unit. The TGC and CPOx devices (see Fig. 2) are modeled individually. Thermal effects within each model are captured with quasi 1-D thermal resistance models. Lumped surface temperatures are assumed within the thermal resistance models where lumped surface definitions are shown in Fig. 6. The CPOx and TGC models share common boundaries with the CFD and tube model. At these model interfaces, the UDF extracts and exchanges the thermodynamic state, thus coupling the CPOx and TGC models to the SOFC system model (see Fig. 3). For example, the state of preheated fuel/air entering the CPOx reformer is first extracted from the CFD model and used as an input to the CPOx model. The state of reformate within the fuel plenum is extracted and used as the anode flow inlet condition for the 1-D tube model. The CPOx and the TGC models provide a critical coupling of the fuel reforming

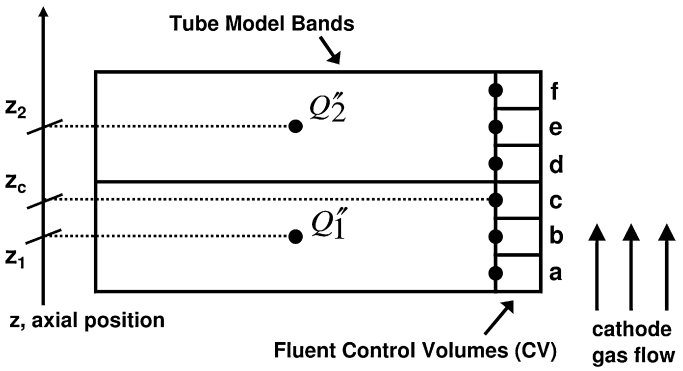

Fig. 5. Linear interpolation of variable passing from 1-D tube model to 3-D Fluent model.

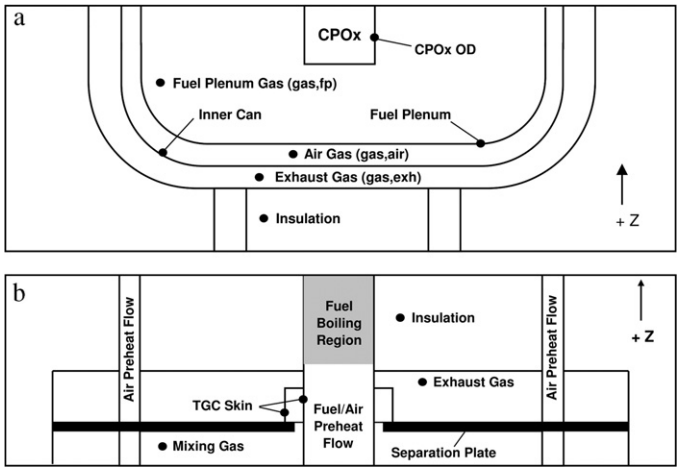

Fig. 6. Lumped surface definitions in both the CPOx (a) and TGC (b) thermal resistance models. Conduction heat transfer is modeled through solids (expect CPOx and TGC components) yielding an inner and outer lumped surface temperature on solids. Only one surface node is shown on solid surfaces for clarity.

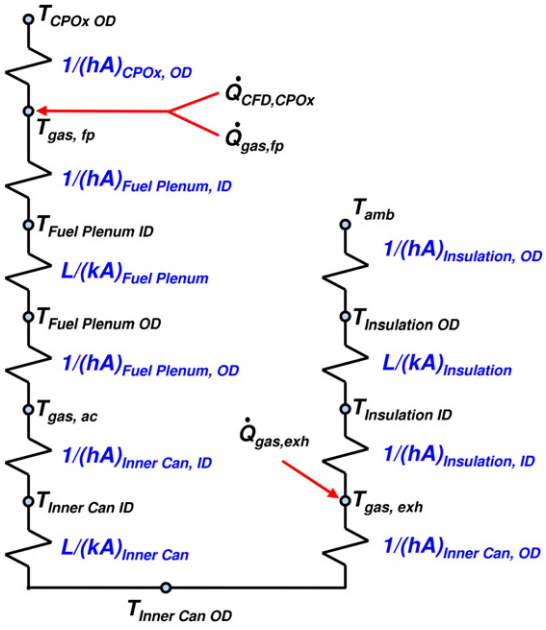

Fig. 7. CPOx model thermal resistance network.

and the combustion of unspent fuel to the CFD and tube models, thereby capturing the full performance of the overall SOFC system.

2.5.1. CPOx model

The CPOx reformer is a porous disc with a catalyst coating that reforms the preheated fuel/air mixture leaving the CFD domain. A gaseous mixture of fuel, n-hexadecane, and air is converted to syngas via the overall reaction below.

$$C_{16}H_{34} + 8(O_2 + 3.76N_2) \Leftrightarrow 16CO + 17H_2 + 30.0N_2 \quad (8)$$

It is essential to couple a CPOx model to accurately predict system performance. As an example, conditions within the CFD model, such as extent of fuel/air preheat, directly effect the temperature of reformate leaving the CPOx which subsequently enters the anode of the tube model. The CPOx model domain extends from the bottom of the inlet tube-sheet to the bottom of the system insulation (see Fig. 2) and also includes anode gas flow through the non-active tube lengths within the inlet tube-sheet, as discussed in Section 2.4.4. A quasi 1-D thermal resistance model created in Python [14] is applied to the CPOx domain, as shown in Fig. 7, to capture thermal and fluid interactions occurring in/around the CPOx reformer. Reformate leaving the CPOx reformer is assumed to be in chemical equilibrium [15,16]. Within the thermal resistance model is a CPOx reformer, fuel plenum wall, fuel plenum gases, an inner can that separates the air channel from the exhaust channel, air and exhaust gases located within the channels, and insulation as shown in Fig. 6.

2.5.1.1. Thermal resistance model. Convection and conduction heat transfer are modeled within the CPOx region assuming lumped surface temperatures on all components (see Fig. 6). The surface temperature of the CPOx reformer is taken as the average of the inlet and outlet gas temperatures. Thermal coupling within the CPOx domain is accomplished through a series of energy balances on all surfaces and the gases within the fuel plenum and exhaust channel. The convective heat transfer, $\dot{Q}_{conv,i}$, from any surface i is calculated as:

$$\dot{Q}_{conv,i} = hA_i\left(T_i - T_{gas,j}\right) \quad (9)$$

where T_i is the lumped temperature and A_i is the area of surface i and $T_{gas,j}$ is the free stream temperature of gas in contact with surface i. A convective heat transfer coefficient, h, common to all surfaces i, within the CPOx control volume is used. In order to capture the presence of radiation heat transfer without the added complexity of solving non-linear equations, an effective heat transfer coefficient is used (Eq. (10)). A value of 100 W m^{-2} K^{-1} is chosen to represent heat transfer throughout the CPOx domain. While there is uncertainty surrounding this value, the heat transfer coefficient is seen as a tuning parameter which can be varied in order to match model predictions to experimental data. Future publications will also investigate the sensitivity of system parameters to the chosen CPOx heat transfer coefficient.

$$h = h_{conv} + h_{rad} = 100\,\mathrm{W\,m^{-2}\,K^{-1}} \quad (10)$$

Conduction, $\dot{Q}_{cond,i}$, through solid regions i is calculated as:

$$\dot{Q}_{cond,i} = (T_{i,inner} - T_{i,outer}) \cdot \left(\frac{L_i}{k_i A_{avg,i}}\right)^{-1} \quad (11)$$

where $T_{i,inner}$ and $T_{i,outer}$ are the surface temperatures of solid region i, $A_{avg,i}$ is the average surface area between the inner and outer surfaces of solid region i and L_i is the thickness of the solid region.

Reformate gas flow within the fuel plenum cavity and exhaust channel gas flow is assumed to be perfectly mixed. Because gas flows entering the CPOx domain are not at the perfectly mixed gas temperature, thermal energy exchange is captured by $\dot{Q}_{gas,i}$ as follows,

$$\dot{Q}_{gas,i} = \dot{m}_i Cp_i\left(T_{i,in} - T_{gas,i}\right) \quad (12)$$

where $\dot{Q}_{gas,i}$ is the amount of thermal energy added at each gas volume node i, $(T_{i,in} - T_{gas,i})$ is the temperature difference between the gas entering the volume and the perfectly mixed temperature, $\dot{m}_i$ is the flow rate, and Cp_i is the specific heat calculated at the average of the inlet and perfectly mixed temperatures. Anode gas flow inside the inactive tube ends is added to the fuel plenum cavity volume. During the physical steady-state operation of this system, all air flowing down the recuperator enters the cathode and no air flow enters the air channel surrounding the fuel plenum; therefore, there is no thermal energy source, $\dot{Q}_{gas,i}$, in the air channel, Fig. 7.

2.5.1.2. Model integration to system model. The thermodynamic state of all flow inlets to the CPOx model which include the fuel/air preheat and exhaust leaving the recuperator are extracted from FLUENT via the UDF. The equilibrium CPOx reformate is sent as the anode inlet condition for the stack. A perfectly mixed condition is applied within the fuel plenum; therefore, reformate is uniform in temperature, pressure, and composition entering the anode of all tubes within the bundle. Besides flow interfaces, there are also solid interfaces at the CPOx boundary between the CFD and tube models. Adiabatic boundary conditions are applied at the interfaces of the system insulation and the inner can wall. The top of the fuel plenum cavity as well as anode gas channels in inactive tube sections are bound by surfaces within the CFD model. At these CFD surfaces a convective thermal boundary condition is applied with h = 100 W m^{-2} K^{-1} and a free stream temperature equal to the fuel plenum gas temperature as calculated in the CPOx thermal resistance model. The total heat transfer at the interface calculated by the CFD model, $\dot{Q}_{CFD,CPOx}$, is added to the energy balance at the fuel plenum gas node within the CPOx thermal model.

2.5.2. TGC model

Thermal interactions in/around the TGC are captured with a thermal resistance network following the same principles used in the CPOx model. Unlike the CPOx model, the TGC model assumes complete combustion [1,3] of any unspent fuel leaving the stack. In addition, the TGC must capture the preheating of two process gas streams, (i) air bound for the cathode and (ii) a mixture of fuel and

Table 2
Simulation parameters.

Fuel/air inlet	
Fuel type	$C_{16}H_{34}$
T/°C	40
P/kPa	92.65
Air inlet	
T/°C	20
P/kPa	84.37
Stack	
j_{avg}/A cm^{-2}	0.349
System	
CPOx: O/C	1.1
λ_{air}	2.55

air bound for the CPOx. Details of the TGC model development can be found in Appendix A.

3. Simulation

The objective of the simulation is to demonstrate the capabilities and utility of the developed, high-fidelity SOFC modeling tool. To begin, an energy and mass balance are calculated to check the integrity of the system model. System level results are presented illustrating the capability of the model to highlight ineffective system architectures. Next, a detailed stack analysis illustrates the non-uniform performance within the stack and the usefulness of the model to stack developers.

The nominal gross electric power output of the SOFC system is 650 W. Thus, the electrical power target for the simulation was ±10% of the nominal value. To vary bundle power without changing inlet conditions, the insulation thickness around each modeling domain (CFD, CPOx, and TGC) was varied by a common factor. Utilizing a 2X insulation factor, the system model resulted in 637 W gross electrical power with insulation 30, 24, and 31.5 mm thick surrounding the CFD, CPOx, and TGC domains, respectively.

3.1. Simulation input parameters

The symmetric tube bundle, shown in Fig. 1, was simulated yielding 19 independent tube simulations. Inlet conditions and system parameters applicable to a 650 W stack were supplied by the SOFC developer and are summarized in Table 2. The amount of stoichiometric air, λ_{air}, for this hexadecane fueled system is calculated using the following,

$$\lambda_{air} = \left(\frac{\dot{n}_{O_2}}{24.5 \cdot \dot{n}_{C_{16}H_{34}}} \right)_{\text{system inlet}} \quad (13)$$

Ambient conditions of T_{amb} = 20 °C and P_{amb} = 83 kPa surround the system insulation. The thermal boundary imposed to the outer insulation surface surrounding the system is convective with h = 10 W m^{-2} K^{-1}. In addition to convection, a radiation pathway is imposed at the insulation periphery in the CFD model, but the addition of radiation has little to no effect because of the low insulation skin temperature, 50 °C.

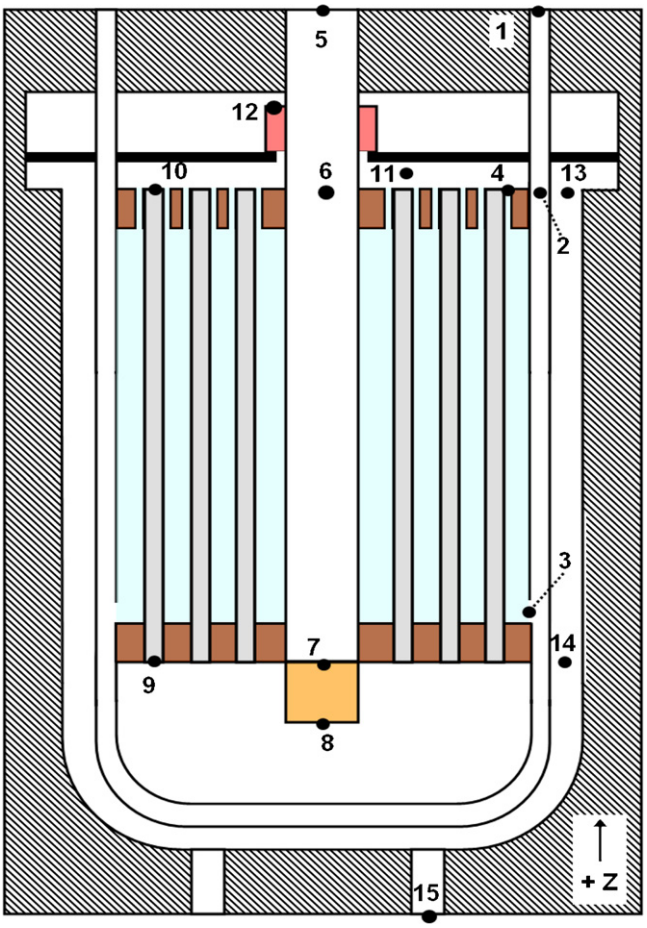

Fig. 8. System process statepoint locations.

3.2. Verification of system model integrity – energy and mass residuals

The integrity of the system model was verified by performing mass and energy balances around the system and component models. The resulting residuals are shown in Table 3. The total energy residual on the system is 0.50% of total energy input into the system and the combined CFD plus tube bundle energy residual is less than 2% of SOFC stack power. Mass balances across the TGC and CPOx models with a slight imbalance seen in the CFD plus tube bundle model. This mass imbalance is very low being less than 5% of the relatively small O_2 mass consumed in the stack.

3.3. Simulation of the SOFC system

The SOFC power generator is simulated operating on a liquid hexadecane fuel. Simulation results are presented for both the overall system and for the tube bundle. Table 4 presents the thermodynamic states throughout the system with statepoints corresponding to Fig. 8. The energy content at each statepoint is the

Table 3
Energy and mass residuals.

Model	Energy residual			Mass residual		
	Value/W	% Total inlet energy	% SOFC power	Value/g s^{-1}	% Total inlet flow	% O_2 consumed in stack
System	14.9	0.5%	2.3%	−3.4E−4	0.01%	4.2%
CFD + tube bundle	12.4	0.4%	1.9%	−3.4E−4	0.01%	4.2%
TGC region	1.9	0.1%	0.3%	0.0	0.00%	0.0%
CPOx region	0.6	0.0%	0.1%	0.0	0.00%	0.0%

Table 4
System statepoints.

Statepoint	T/°C	P/kPa	Flowrate/g s^{-1}	Molar composition								E/W
				H_2	CO	CH_4	$C_{16}H_{34}$	CO_2	H_2O	O_2	N_2	
1	20	84.37	2.410	0.0	0.0	0.0	0.00	0.0	0.0	0.21	0.79	0
2	111	84.37	2.410	0.0	0.0	0.0	0.0	0.0	0.0	0.21	0.79	223
3	668	84.25	2.410	0.0	0.0	0.0	0.0	0.0	0.0	0.21	0.79	1664
4	699	84.22	2.330	0.0	0.0	0.0	0.0	0.0	0.0	0.19	0.81	1695
5	40	92.65	0.402	0.0	0.0	0.0	0.02	0.0	0.0	0.21	0.77	3010
6	294	92.65	0.402	0.0	0.0	0.0	0.02	0.0	0.0	0.21	0.77	3157
7	422	92.65	0.402	0.0	0.0	0.0	0.02	0.0	0.0	0.21	0.77	3227
8	1218	92.65	0.402	0.24	0.24	0.0	0.0	0.01	0.02	0.0	0.50	3226
9	816	84.22	0.402	0.24	0.24	0.0	0.0	0.01	0.02	0.0	0.50	2974
10	718	84.22	0.483	0.10	0.10	0.0	0.00	0.14	0.16	0.0	0.50	1633
11	716	84.22	2.813	0.02	0.02	0.0	0.0	0.03	0.03	0.15	0.76	3371
12	999	84.22	2.813	0.0	0.0	0.0	0.0	0.05	0.05	0.13	0.77	3345
13	868	83.27	2.813	0.0	0.0	0.0	0.0	0.05	0.05	0.13	0.77	2889
14	656	83.22	2.813	0.0	0.0	0.0	0.0	0.05	0.05	0.13	0.77	2177
15	682	83.00	2.813	0.0	0.0	0.0	0.0	0.05	0.05	0.13	0.77	2264
Power												637
Heat loss												94

summation of (i) thermal energy released when cooled to the ambient temperature, (ii) chemical energy released with the oxidation of any fuels present, and (iii) latent energy associated with condensing water if present.

System air is preheated from 20 °C to 668 °C before entering the cathode at statepoint 3. The fuel/air gas mixture is preheated from 40 °C to 422 °C (statepoint 7) prior to entering the CPOx reformer and subsequently enters the anode at 816 °C (statepoint 9). The bundle at an average temperature of 745 °C produces 637 W of gross power at 43.3 V and 14.72 A. TGC exhaust gases enter the recuperator at 868 °C (statepoint 13), leaving the recuperator at 656 °C (statepoint 14), and finally are heated slightly while flowing through the CPOx domain leaving the system at 682 °C (statepoint 15). The co-flow recuperator leads to a high system exhaust temperature. Of the 3.01 kW of energy entering the system, 75% is convected away through exhaust gases with 21% converted to dc electrical power in the SOFC tube bundle. Conductive heat loss through system insulation only accounts for 3% of total system energy input. Table 5 highlights the predicted operating conditions of the system utilizing the following definitions,

$$U_F = \frac{\left(\dot{n}_{H_2}\right)_{\text{stack consumed}}}{\left(4\dot{n}_{CH_4} + \dot{n}_{H_2} + \dot{n}_{CO}\right)_{\text{anode inlet}}} \tag{14}$$

$$U_{ox} = \frac{\left(\dot{n}_{O_2}\right)_{\text{stack consumed}}}{\left(\dot{n}_{O_2}\right)_{\text{cathode inlet}}} \tag{15}$$

$$\eta_{\text{system}} = \frac{P_{\text{DC,stack}}}{(\dot{n}_{\text{fuel}} \cdot \text{HHV}_{\text{fuel}})_{\text{system inlet}}} \tag{16}$$

$$\eta_{\text{SOFC}} = \frac{P_{\text{DC,stack}}}{(\dot{n}_{\text{fuel}} \cdot \text{HHV}_{\text{fuel}})_{\text{anode inlet}}} \tag{17}$$

where U_F is the fuel utilization and U_{ox} is the oxygen utilization within the stack, η_{system} and η_{SOFC} are the system and stack efficiencies, respectively. $P_{\text{DC,stack}}$ is the DC power output from the stack and found in both efficiency definitions because blowers, pumps, and power conditioning are not modeled in this study. The relatively low system efficiency registered in this simulation is consistent with SOFC developer performance and substantially affected by the low fuel utilization.

Table 5
System operating conditions.

Operating conditions	
$P_{\text{cathode, avg}}$/kPa	84.24
$P_{\text{anode, avg}}$/kPa	84.22
U_F	0.56
U_{Ox}	0.14
η_{SOFC}	25.1%
η_{system}	21.1%

The predicted CPOx reformer exhaust temperature, 1218 °C, could lead to sintering within the reformer. Heat loss from the reformer is directly coupled to the estimated reformer skin temperature used within the thermal resistance network. Averaging inlet and outlet gas flow temperatures to estimate the CPOx skin temperature adds uncertainty to the thermal model. Experimental temperature profile data of the reformer would remove the uncertainty surrounding the CPOx skin temperature and predicted CPOx exhaust temperature.

3.4. Tube bundle results

Tube bundle performance is investigated with the aim of understanding tube temperature and oxygen distributions, flowfield characteristics, and identification of potential model reduction methods by strategic groupings of tubes.

3.4.1. Tube performance groupings

For every tube in the bundle, radiation is observed to be the dominant heat transfer mechanism for stack cooling at the outer tube surface. The annular stack can surrounding the bundle separates the cathode gases from the relatively cold air being preheated in the recuperator. The stack can has a non-linear temperature distribution with a maximum of 691 °C, a minimum of 523 °C, and a 621 °C average temperature. With the average bundle temperature at 745 °C, a large temperature driving force for radiation heat transfer to the stack can exists. Tubes with larger radiation view factors to the stack can are observed to transfer a proportionally larger amount of radiation thermal energy causing their temperatures to decrease along with tube power. Power disparities are observed within the bundle as cell power ranges from 7.6 to 10.8 W with an average of 9.7 W.

Power disparities are largely due to a strong functional relationship between the power output of a tube and the view factor from the tube to the stack can. This relationship is shown in Fig. 9 where the tubes are arranged in increasing power output on the x-axis. Tubes with similar view factors to the stack also have very similar power outputs. For the bundle configuration under study, seven view factor groupings exist which lead to seven tube power groupings. Groupings 6 and 7 could be combined into a single power

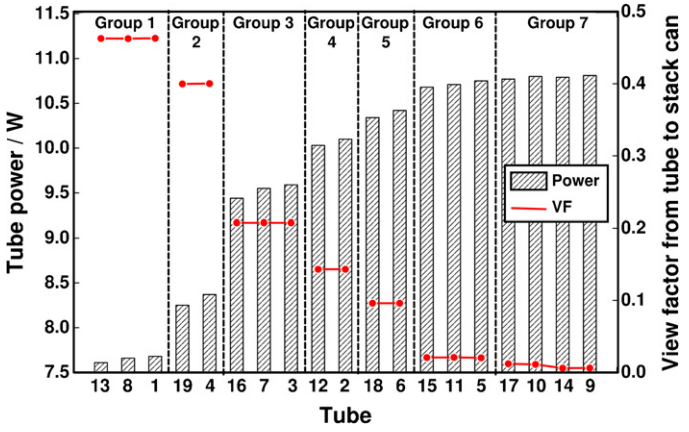

Fig. 9. Plot of tube power and view factor from tube to stack can surface for every tube in bundle. Arranged in groupings of similar view factors.

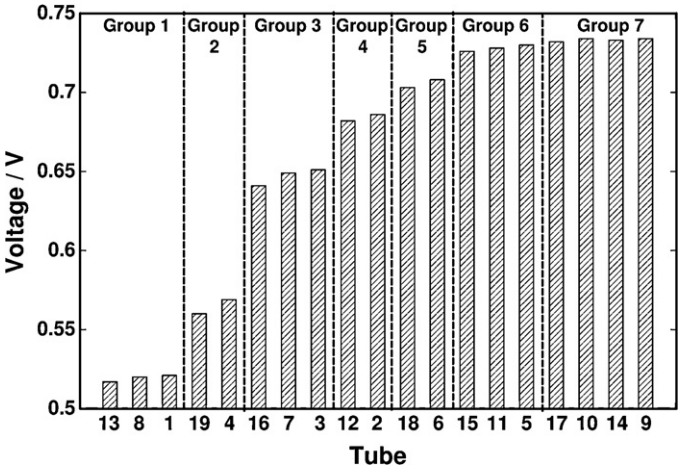

Fig. 11. Operating voltage of every tube within bundle.

group, but they are left as distinct groups because of differences in axial temperature profiles which is discussed further in Section 3.4.2. Variations in tube performance point to the potential for substantial inaccuracy in stack power prediction if the performance of a single tube is extrapolated to emulate the performance of an entire tube bundle. Resulting power groupings suggest at least six if not seven tube simulations are required in order to predict the performance of the stack, where each tube simulation requires a unique set of thermal boundary conditions.

The dominance of radiation in the bundle is explicitly illustrated in Fig. 10 where individual tube heat losses have been averaged within power groupings. For tubes located closer to the stack radial center, outer radial periphery tubes act as radiation shields effectively blocking the view to the relatively cold stack can. This is convincingly seen in Fig. 10 where the outer radial tubes (groups 1 and 2) have the greatest percentage of radiation loss, 87–92%, compared to inner radial tubes (groups 6 and 7) where 66–67% of heat transfer is due to radiation. Because of this shielding, tube power groupings are also a function of radial tube location as clearly shown in Fig. 9 where tubes at the inner radii produce the greatest power and tubes at the outer bundle radii produce the lowest power.

Because the stack is wired in electrical series, cell voltage varies throughout the bundle as shown in Fig. 11. Cell voltages vary from 0.52 to 0.73 V at the lowest power and highest power tubes, respectively. Voltages lower than 0.6 V occurring in tube groupings 1 and 2 are of concern as oxygen ions may begin to oxidize Ni in the anode. Further research needs to determine the voltage limit to avoid Ni oxidization. If tube groups are below the voltage limit, each cell within a grouping could be wired in series and each grouping could be wired in parallel. Thus, the current load for each grouping could be varied in order to maintain acceptably high cell voltages.

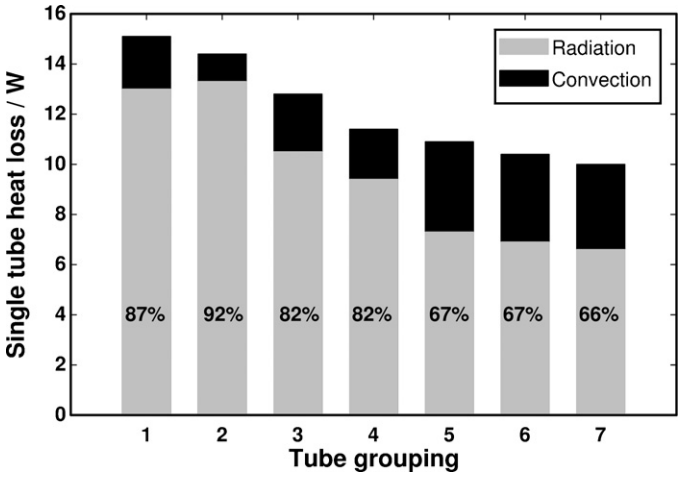

Fig. 10. Heat transfer pathways in tube groupings. Percentage of radiation written on graph.

3.4.2. *Temperature and O_2 axial profiles*

Area-averaged axial tube temperature profiles, $T(z)$, along with surface oxygen molar concentrations, $X_{O_2}(z)$, are shown for every tube in Fig. 12. Fig. 12 is organized utilizing the power groups defined in Fig. 9. As tube power is a strong function of temperature, tube temperatures within a given power group remain within 10 °C of each other. Conduction from the relatively hot CPOx region (816 °C anode gas inlet) combined with high localized current density contribute to the maximum cell temperature at the anode inlet. Because air enters the cathode at a relatively cold temperature of 668 °C, all tube temperatures initially decrease with increasing axial distance. Due to their close proximity to the stack can, tubes in groups 1 and 2 continue to drop in temperature with a small increase near the anode outlet due to the heat supplied by the TGC. All remaining tubes in the bundle produce enough thermal energy due to irreversibilities in the electrochemical reactions to increase their temperatures after the initial temperature decrease. The ΔT between the bundle and stack can increases in the direction of cathode and anode flow because cold oxidant enters the recuperator near the anode and cathode outlets. Radiation exchange overcomes internal tube heat generation causing temperatures to decrease at the local temperature maximum occurring approximately halfway down the length of the bundle.

Surface oxygen concentrations are dependent on bulk convective cathode mixing as well as diffusion. Oxygen diffusion from the bulk cathode to the tube surface is driven by the current produced by a tube. With the total current, 14.72 A, of each tube held constant, the sum of O_2 diffusion to the tube surface is constant for each tube. Localized current densities are directly proportional to tube temperature as seen in Fig. 12b. As the temperature of group 4 increases, O_2 concentration decreases at an increased rate due to a higher localized current density. Interestingly, surface O_2 concentrations do not decrease in the flow direction along the length of the cell. The 3-D cathode model captures increases in axial O_2 concentrations due to variations in convective mixing. For example, O_2 concentrations increase near the cathode outlet because cathode gases exit through concentric circle cut-outs surrounding each cell in the outlet tube-sheet. Combining the quasi-radial bun-

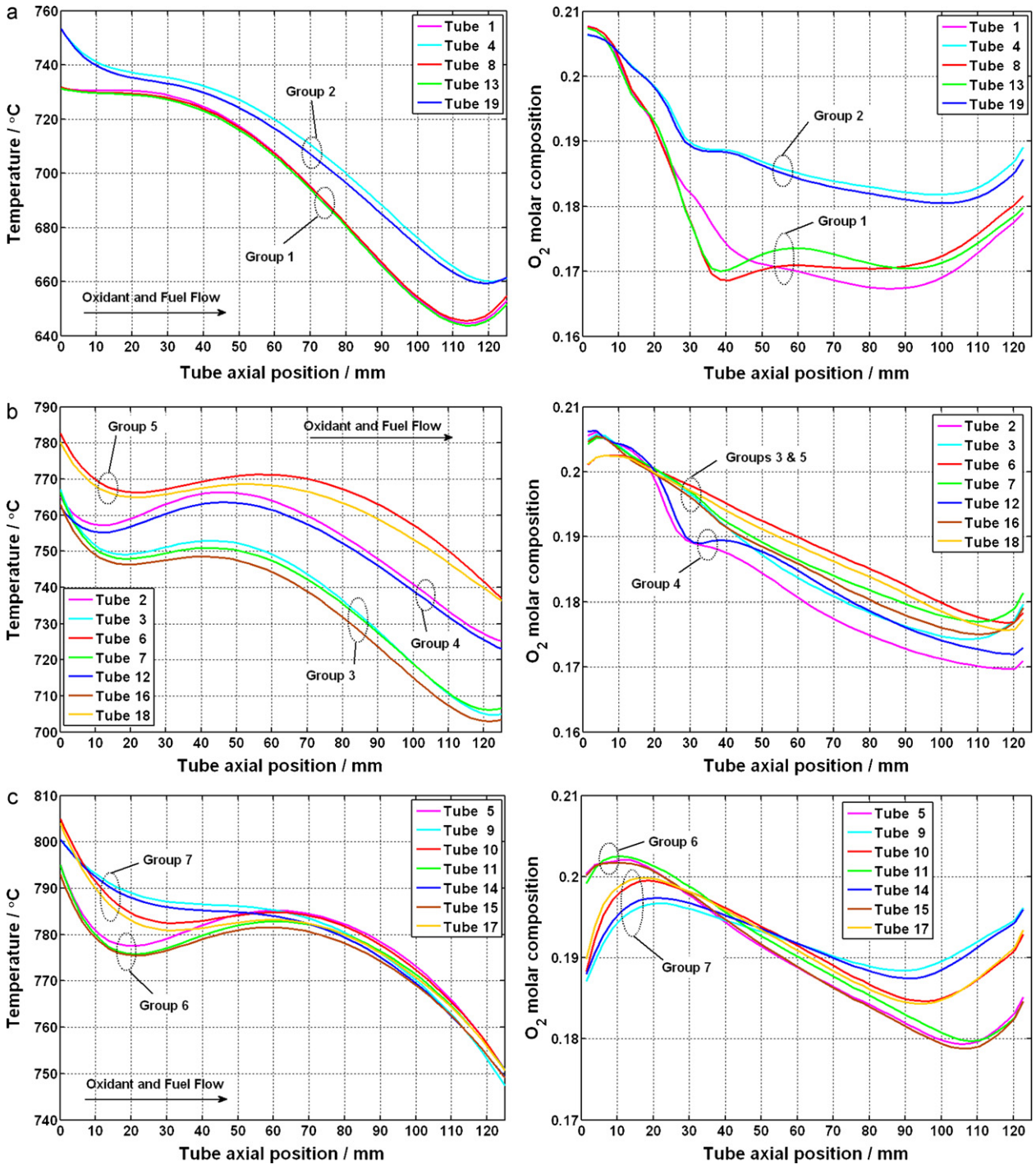

Fig. 12. Temperature and surface oxygen molar concentration profiles of every tube in bundle. Tubes grouped based on power groupings in Fig. 9. (a) Tube groupings 1 and 2. (b) Tube groupings 3, 4, and 5. (c) Tube groupings 6 and 7.

dle symmetry and the radial cathode inlet to the bundle, variations in convective mixing between cells is primarily a function of radial position. Tube powers were also shown to have a radial dependence which explains why O_2 concentration profiles within power groupings are very similar.

3.4.3. Contours plots and cathode oxidant pathlines

Contour plots of bundle temperature and surface oxygen concentration are shown in Fig. 13. In both figures cathode gases enter through the dark ring at the bottom of the bundle. Cathode gases flow in the positive *z*-direction and exit the bundle through concentric circle cutouts in the outlet tube-sheet. Anode gases also flow in the positive *z*-direction in a co-flow configuration. Symmetric stack results are mirrored to show half of the bundle in Fig. 13. Contours of tube temperature are shown on the left quarter with contours of surface oxygen molar concentration shown on the right quarter. Temperature contours illustrate the radiation shielding effect outer periphery tubes have on inner periphery tubes. The inner periphery ring of tubes is relatively hot with a uniform temperature distribution. Cold zones are seen at the outer periphery tubes

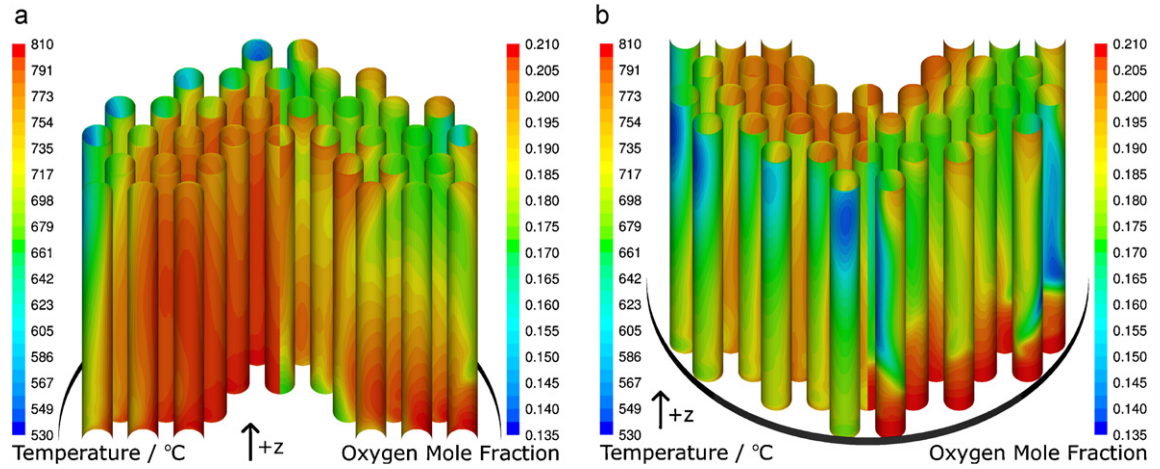

Fig. 13. Contour plots of surface oxygen molar concentrations on the right quarter and tube temperatures on the left quarter. (a) Looking down onto interior aspect of bundle. (b) Looking down onto exterior aspect of bundle.

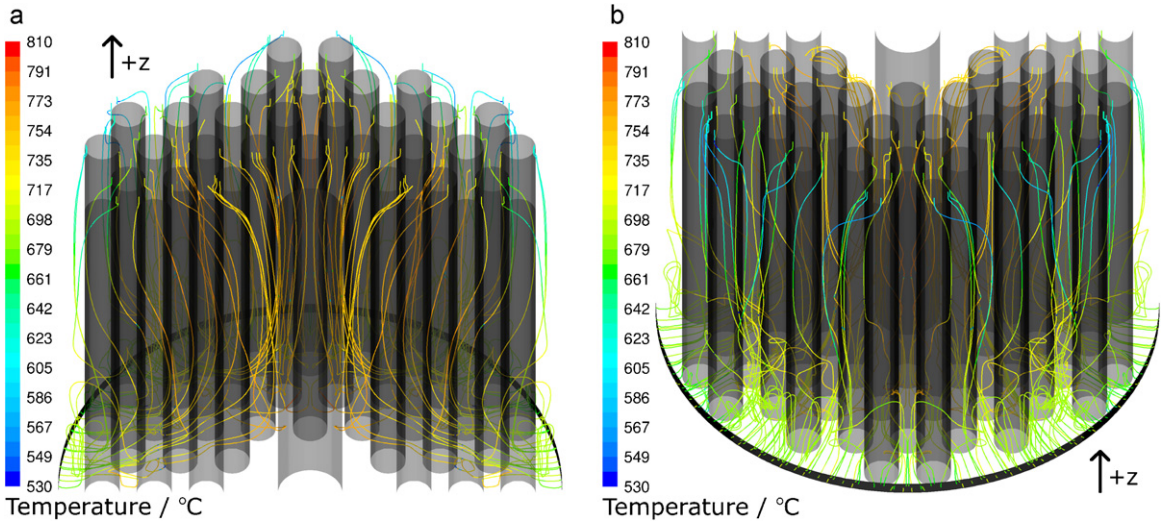

Fig. 14. Pathlines with cathode colored by temperature. Tube bundle and central fuel preheat tube walls shown in black. (a) Looking down onto interior aspect of bundle. (b) Looking down onto exterior aspect of bundle.

caused by their close proximity to the stack can wall as well as by low cathode mixing. As each tube consumes the same amount of O_2 (constant cell current), low O_2 concentrations at outer periphery tubes are the result of low convective mixing not O_2 diffusion at the cathode. A further indicator of ineffective cathode mixing is demonstrated in the cathode particle pathlines colored by temperature in Fig. 14. To reach the outer periphery tube surfaces, the oxidant needs to turn 180° after entering the cathode. Pathlines indicate the majority of oxidant flows interior to the bundle unable to overcome initial inward radial momentum and reach the outer periphery tubes.

4. Conclusion

A powerful tubular SOFC system design and simulation tool has been developed. A detailed stack model coupling CFD to a 1-D electrochemical tubular cell model allows one to see how stack geometries affect variations in tube performance. By integrating a recuperator, tail-gas combustor, and catalytic partial oxidation reformer to the detailed stack model, thermal interactions between BoP and the SOFC stack are captured in the system level model. Model results can point fuel cell developers to more effective system architectures and optimal operating conditions with the goal of increasing system efficiencies by optimizing the thermal coupling between BoP and the SOFC stack.

The model capabilities were explored through simulation of a highly integrated tubular SOFC system for small (~1 kW) mobile applications. The simulation predicts a fuel conversion efficiency of 21%, where 75% of the input fuel energy is convected away with the exhaust stream, and the remaining 3% lost through heat transfer to the environment. With 75% of energy lost in the exhaust stream, model results highlight the ineffective use of a co-flow recuperator, and a counter-flow recuperator is a recommended design improvement. With ineffective preheating of oxidant, cathode gases are 148 °C colder than anode gases entering the stack causing a large decrease in tube temperatures near the cathode inlet. Unlike planar stacks, convective cooling is not the dominate mechanism for heat transfer within the stack; therefore, a large ΔT is not required of cathode gases entering the bundle.

Simulation results point to radiation heat transfer as the dominate mechanism of stack cooling within tubular stacks. Radiation accounts for 62–93% of total heat rejection from the external tube

surface. The dominance of radiation leads to a strong relationship between the power output of a tube and the view factor from the tube to the relatively cold stack can wall. The bundle under study results in seven tube groupings based on similar view factors to the stack can. These seven view factor groupings correspond to seven power groupings. Tube performance groupings yield insight into potential reduced-order modeling strategies of such geometric configurations. One such strategy would be to simulate stack performance based on tube groupings rather than the extrapolation of a single electrochemical tube. This strategy would require a unique set of thermal boundary conditions to be extracted from the detailed CFD analysis for each tube grouping.

An enormous amount of information for detailed stack design is also available from this modeling tool. Contour plots of stack temperatures reveal relatively hot and uniform tubes at the inner periphery but cold zones develop at the outer periphery of the bundle. Cathode mixing is also seen to be relatively low with low oxygen concentrations at the outer periphery, low power tubes. Non-uniformities within the stack lead to power disparities amongst cells. As cell power varies from 7.6 to 10.8 W, the current stack design leaves room for improvement. It is recommended that tubular stacks be configured such that the variation in view factors from cells to the stack surroundings is minimized. While the simulation tool was implemented for small-scale tubular SOFCs, it should be noted that the modeling approach employed is applicable to a wide range of SOFC systems.

Acknowledgments

The authors would like to thank Dr. Robert Kee for his helpful suggestions, illustrations, and for facilitating the collaborative effort with ANSYS-FLUENT. Funding for this work was provided by the U.S. Department of Energy, Office of Energy Efficiency & Renewable Energy (EERE) under contract number DE-FG36-08GO88100.

Appendix A. TGC model

The TGC is a porous annular disk where unspent fuel from the stack is oxidized with cathode exhaust gases. TGC exhaust then enters the CFD domain at the recuperator hot flow inlet. As with the CPOx model, it is essential to couple the TGC model to the system. As an example, if the tube model predicts low stack power, an increase in unspent fuel will increase the TGC exhaust temperature which indirectly increases the temperature of air leaving the recuperator, i.e. entering the cathode. A higher cathode inlet temperature acts to increase tube temperatures and power output; therefore, TGC coupling acts to regulate stack power. The TGC model domain extends from the top of the outlet tube-sheet to the top of the system insulation (see Fig. 2) and also includes the anode gas flow through the inactive tube lengths within the outlet tube-sheet, as discussed in Section 2.4.4. A quasi 1-D thermal resistance model created in Python is applied to the TGC domain, as shown in Fig. A.1, to capture thermal and fluid interactions associated with the TGC. Complete combustion is assumed within the TGC [1,3]. The TGC domain consists of a mixing region where stack cathode and anode exhaust gases mix, a combustor, combustor exhaust cavity, fuel/air preheat tube flow, air preheat tube flow, and a separating plate that separates the mixing region from the TGC exhaust cavity, as shown in Fig. 6.

A.1. Thermal resistance model

Convection and conduction heat transfer are modeled in the same manner as in the CPOx model where all surfaces are at lumped temperatures within the TGC control volume (see Fig. 6 for geometry). The surface temperature of the TGC is taken as the average of the inlet and outlet gas temperatures. An effective heat transfer coefficient is used in the TGC domain with the same value as used in the CPOx model (see Eq. (10)). A perfectly mixed gas condition is applied to the mixing region and the TGC exhaust gas cavity as given in Eq. (12).

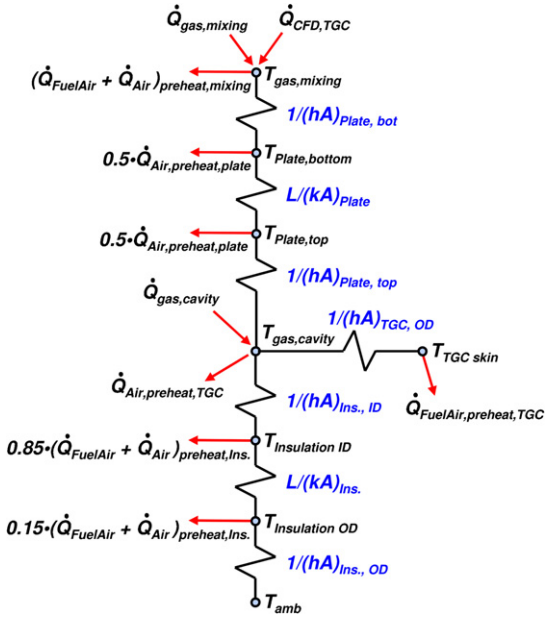

Fig. A.1. TGC model thermal resistance network.

A.2. System air flow preheat modeling

The TGC domain also has pipe flows used to preheat system streams of fuel/air and air. Pipe flow is not perfectly mixed, and the conductive resistance of the solid pipes is assumed negligible. There are four air preheat flow tubes within the TGC domain (only two seen in cut view of Fig. 6). A turbulent ($Re \approx 5000$) pipe flow Nusselt number relation was used in creating a mass flow rate functional dependence for the heat transfer coefficient within air preheat tubes.

$$h_{\mathrm{air,preheat}} = 59664 \cdot \dot{m}_{\mathrm{air}}^{0.887} \tag{A.1}$$

where $\dot{m}_{\mathrm{air}}$ is the mass flow rate ($\mathrm{kg\,s^{-1}}$) of air per air preheat tube.

The air flow tubes pass through four regions of the TGC domain, namely the insulation, TGC exhaust cavity, separation plate, and mixing region. The magnitude of heat transfer from each region to preheat air flow is calculated by combining energy balances and rate equations applied at each region the air flow tubes pass through. The rate of heat transfer in each region is defined as:

$$\dot{Q}_{\mathrm{air},i} = h_{\mathrm{air,preheat}} A_{\mathrm{air},i} \left[T_{\mathrm{avg},i} - T_{\mathrm{air,avg},i} \right] \tag{A.2}$$

where $\dot{Q}_{\mathrm{air},i}$ is the thermal energy transferred into the air flow traveling through tube region i having surface area $A_{\mathrm{air},i}$ and $T_{\mathrm{avg},i}$ is an average temperature representing the air flow tube in region i. When the tube borders a solid region, $T_{\mathrm{avg},i}$ is the average between the inner and outer solid surface temperatures. When the tube borders a gas cavity, $T_{\mathrm{avg},i}$ is the perfectly mixed gas temperature. Air flow temperatures are calculated at the periphery of every region that the flow tube intersects; therefore, $T_{\mathrm{air,avg},i}$ is the average between the inlet, $T_{\mathrm{air,in},i}$, and outlet, $T_{\mathrm{air,out},i}$, air temperature within region i. Energy balances are applied to air flow in each region i as:

$$\dot{Q}_{\mathrm{air},i} = \dot{m}_{\mathrm{air}} Cp_{\mathrm{air}} \left(T_{\mathrm{air,out},i} - T_{\mathrm{air,in},i} \right) \tag{A.3}$$

where Cp_{air} is the specific heat representing air within the preheat tube and is evaluating at the average temperature of air into and out of the entire TGC domain.

A.3. System fuel/air flow preheat modeling

Fuel/air preheating occurs in the centrally located fuel inlet flow tube. In the physical system, fuel is injected (mixing with air) into the preheat tube by an atomizing spray nozzle where the nozzle tip is located at the outer periphery of the insulation. A physical spray nozzle is not modeled within the TGC, but to simulate this boundary condition, a mixture of liquid fuel and gaseous air enter the preheat tube at a common temperature. Within the tube, atomized fuel droplets are rapidly vaporized. Heating of the vaporizing fuel and gaseous air mixture is modeled by considering the air and liquid fuel components separately. An energy balance coupled to a rate equation calculates the tube area where vaporization occurs. $\dot{Q}_{f/a,vap}$ is the total energy required to first sensibly heat liquid fuel and gaseous air to the boiling temperature of the fuel and the latent energy required to completely vaporize the fuel.

$$\dot{Q}_{f/a,vap} = \dot{m}Cp\left(T_{boil} - T_{f/a,in}\right)_{air} + \dot{m}\left[h_{fg} + Cp_{liq}\left(T_{boil} - T_{f/a,in}\right)\right]_{fuel} \quad (A.4)$$

where T_{boil} is the boiling temperature of the fuel, $T_{f/a,in}$ is the fuel/air temperature into the TGC domain, and h_{fg} (359 kJ kg^{-1} for n-hexadecane) is the latent heat of vaporization. The mass flow rate of air and fuel entering the preheat tube are $\dot{m}_{air}$ and $\dot{m}_{fuel}$, respectively. $Cp_{liq,fuel}$ is the specific heat of liquid fuel used in calculating the sensible heating of liquid fuel. Cp_{air} is calculated at the average of the inlet and boiling temperatures.

The rate at which $\dot{Q}_{f/a,vap}$ is transferred is calculated as:

$$\dot{Q}_{f/a,vap} = h_{boil}A_{f/a,vap}\left[T_{f/a,tube} - \left(\frac{T_{f/a,in} + T_{boil}}{2}\right)\right] \quad (A.5)$$

where $A_{f/a,vap}$ is the surface area of the fuel/air preheat tube from the inlet to the location of complete fuel vaporization. $T_{f/a,tube}$ is an area averaged temperature of the entire fuel/air preheat tube. A high convective heat transfer coefficient, h_{boil} = 2000 W m^{-2} K^{-1}, is used in the preheat tube as a simplified means to simulate fuel vaporization. Rather than performing a detailed analysis involving non-dimensional groups, h_{boil} is estimated from boiling curves [17]. This rough estimate is appropriate because system level predictions are not sensitive to h_{boil}. For example, an h_{boil} = 1000 W m^{-2} K^{-1} only decreases the fuel/air temperature leaving the TGC domain by 0.7 °C while increasing h_{boil} to 3000 W m^{-2} K^{-1} only increases the fuel/air outlet temperature by 0.3 °C. The fuel/air outlet temperature is not sensitive to h_{boil} because of a low convective coefficient once fuel is vaporized as discussed in the following.

After the fuel has completely vaporized, another set of coupled energy balance and rate equations are applied to determine the extent of fuel/air preheating before entering the CFD domain. In this flow region, a lower convective heat transfer coefficient, $h_{f/a,pre}$ = 9.6 W m^{-2} K^{-1}, is used. $h_{f/a,pre}$ is based on a laminar, $Re \approx 1000$, pipe flow Nusselt number relationship with the assumption of fully developed flow. The amount of sensible heating to the fuel/air gas mixture, $\dot{Q}_{f/a,gas}$, is calculated as:

$$\dot{Q}_{f/a,gas} = \dot{m}_{f/a}Cp_{f/a}\left(T_{f/a,out} - T_{boil}\right) \quad (A.6)$$

where $T_{f/a,out}$ is the temperature of fuel/air gas leaving the fuel/air preheat tube. The combined air and fuel flow rate is $\dot{m}_{f/a}$ and $Cp_{f/a}$ is the specific heat of the mixture calculated at the average outlet and boiling temperatures.

The rate of $\dot{Q}_{f/a,gas}$ is calculated with:

$$\dot{Q}_{f/a,gas} = h_{f/a,gas}A_{f/a,gas}\left[T_{f/a,tube} - \left(\frac{T_{boil} + T_{f/a,out}}{2}\right)\right] \quad (A.7)$$

where $A_{f/a,gas}$ is the surface area of the fuel/air preheat tube from complete fuel vaporization to the outlet of the fuel/air tube. It should be noted that the area averaged temperature of the entire fuel/air preheat tube is used in calculating the driving potential in Eqs. (A.5) and (A.7). The reasoning being that the location of complete fuel vaporization is dependent on system level operating parameters and TGC model dimensions. With the location of complete vaporization unknown, it is difficult to calculate an area-averaged fuel/air preheat tube in both the vaporizing and gaseous fuel sections.

A.4. Model integration into system model

The thermodynamic state of all flow inlets entering the TGC model which include the cathode and anode exhaust are extracted from FLUENT and the tube model via the UDF. The state of preheated fuel/air and preheated air along with the state of TGC exhaust leaving the TGC domain are sent as inlet conditions to the CFD model.

As in the CPOx model, there are also solid interfaces at the TGC boundary between the CFD and tube models. Adiabatic boundary conditions are applied at the interfaces of the system insulation, fuel/air preheat tube, and air preheat tube. The bottom of the mixing region as well as anode gas channels in inactive tube sections are bound by surfaces within the CFD model. At these CFD surfaces a convective thermal boundary condition is applied with h = 100 W m^{-2} K^{-1} and a free stream temperature equal to the mixing gas temperature as calculated in the TGC thermal resistance model. The total heat transfer at the interface calculated by the CFD model, $\dot{Q}_{CFD,TGC}$, is added to the energy balance at the mixing gas node within the TGC thermal model.

References

[1] M. Sorrentino, C. Pianese, J. Fuel Cell Sci. Technol. 6 (2009).
[2] P. Lisbona, A. Corradetti, R. Bove, P. Lunghi, Electrochim. Acta 53 (2007) 1920–1930.
[3] N. Lu, Q. Li, X. Sun, M.A. Khaleel, J. Power Sources 161 (2006) 938–948.
[4] S.H. Chan, O.L. Ding, Int. J. Hydrogen Energy 30 (2005) 167–179.
[5] L. Petruzzi, S. Cocchi, F. Fineschi, J. Power Sources 118 (2003) 96–107.
[6] K.J. Kattke, R.J. Braun, J. Fuel Cell Sci. Technol. 8 (2) (2011), doi:10.1115/1.4002233.
[7] J. Poshusta, et al., Solid Oxide Fuel Cell Systems with Hot Zones and Two-Stage Tail Gas Combustors, Protonex Technology Corporation, US Patent Application 12/006,668 July 9, 2009.
[8] A.M. Colclasure, B.M. Sanandaji, T.L. Vincent, R.J. Kee, J. Power Sources 196 (2011) 196–207.
[9] D.G. Goodwin An open-source, extensible software suite for CVD process simulation, in: M. Allendorf, F. Maury, F. Teyssandier, (Eds)., Chemical Vapor Deposition XVI and EUROCVD 14, volume PV 2003-08, pages 155–162. Electrochemical Society, 2003. see also http://code.google.com/p/cantera/.
[10] Special Metals, INCONEL 600 Data Sheet, product data sheet, Table 3, p. 2, September 2008.
[11] Microtherm International Ltd., Microtherm Insulation Product and Performance Data, product brochure, Table 3, p. 5, June 2001.
[12] F. Calise, M.D. d'Accadia, G. Restuccia, Int. J. Hydrogen Energy 32 (2007) 4575–4590.
[13] J. Jia, A. Abudula, L. Wei, R. Jiang, S. Shen, J. Power Sources 171 (2007) 696–705.
[14] G. van Rossum, Python (Version 2.6) [Computer Software]. Available from: http://www.python.org.
[15] J. Krummenacher, K. West, L. Schmidt, J. Catal. 215 (2003) 332–343.
[16] K. Hohn, T. DuBois, J. Power Sources 183 (2008) 295–302.
[17] F. Incropera, D. DeWitt, T. Bergman, F. Lavine, Fundamentals of Heat and Mass Transfer, Fig. 10.4, 6th ed., Wiley, New York, 2007.